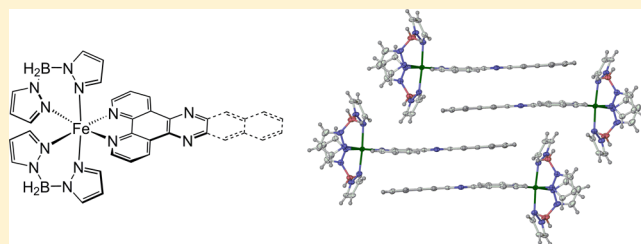


A Homologous Series of $[\text{Fe}(\text{H}_2\text{Bpz}_2)_2(\text{L})]$ Spin-Crossover Complexes with Annelated Bipyridyl Co-Ligands

Rafal Kulmaczewski,[†] Helena J. Shepherd,[‡] Oscar Cespedes,[§] and Malcolm A. Halcrow^{*,†}[†]School of Chemistry, University of Leeds, Woodhouse Lane, Leeds LS2 9JT, U.K.[‡]Department of Chemistry, University of Bath, Claverton Down, Bath, BA2 7AY, U.K.[§]School of Physics and Astronomy, University of Leeds, E. C. Stoner Building, Leeds LS2 9JT, U.K.

Supporting Information

ABSTRACT: Four new iron(II) complexes $[\text{Fe}(\text{H}_2\text{Bpz}_2)_2(\text{L})]$ were prepared (pz = pyrazolyl), where L is dipyrido[3,2-*f*:2',3'-*h*]quinoxaline (dpq), dipyrido[3,2-*a*:2'3'-*c*]phenazine (dppz), dipyrido[3,2-*a*:2'3'-*c*]benzo[*i*]phenazine (dppn), and dipyrido[3,2-*a*:2',3'-*c*](6,7,8,9-tetrahydro)phenazine (dppc). Crystal structures of $[\text{Fe}(\text{H}_2\text{Bpz}_2)_2(\text{dpq})]$, $[\text{Fe}(\text{H}_2\text{Bpz}_2)_2(\text{dppz})]$, and $[\text{Fe}(\text{H}_2\text{Bpz}_2)_2(\text{dppn})]$ all reveal stacks of complex molecules formed through π - π stacking between interdigitated bipyridyl chelate ligands, often with additional intercalated toluene or uncoordinated bipyridyl ligand (dpq). Molecules of $[\text{Fe}(\text{H}_2\text{Bpz}_2)_2(\text{dppc})]$ form a different stacking motif in the crystal, with weaker contacts between individual molecules. Many of the structures also contain channels of disordered solvent, running between the molecular stacks. Despite their different stacking motifs, all these compounds exhibit very gradual thermal spin-crossover (SCO) on cooling, which occur over different temperature ranges but are otherwise quite similar in form. Weak thermal hysteresis in one of these spin equilibria can be attributed to the effects of a change in bipyridyl ligand conformation in the molecular stacks around 150 K, which was observed crystallographically. These results demonstrate that strong mechanical coupling between molecules in a crystal is not sufficient to engineer cooperative SCO switching, if other regions of the lattice are less densely packed.



INTRODUCTION

Although the phenomenon was first elucidated in the 1960s,¹ spin-crossover (SCO) materials continue to be heavily studied,^{2–6} because of their potential applications in display, memory⁷ and actuator devices,⁸ and in nanoscience.⁴ While hundreds of compounds are known to exhibit SCO, the majority being complexes of iron(II), only a handful have the room-temperature switching properties required for device applications.⁹ The temperature and cooperativity of an SCO transition are functions of intermolecular interactions in the crystal lattice, as well as of the molecules themselves. Hence, designing a spin-crossover material with predefined switching properties *de novo* is a problem of crystal engineering as much as coordination chemistry.⁵ As well as being important switchable materials, SCO crystals are also useful models for engineering other types of phase transition into functional molecular crystals.

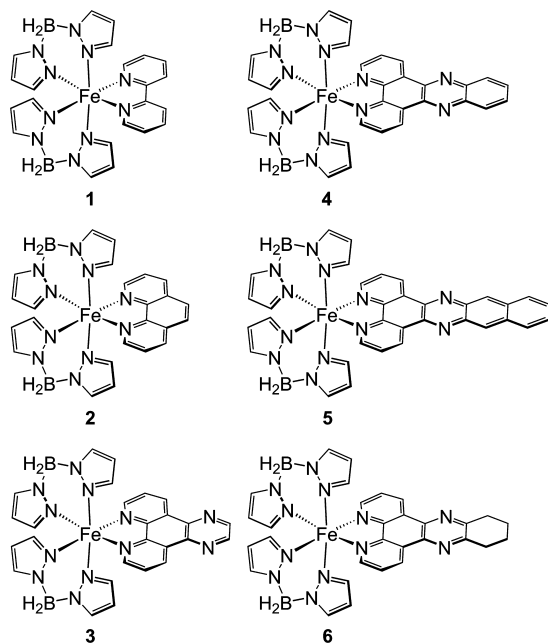
After surveying the literature, we proposed that abrupt, hysteretic spin-transitions can be promoted by molecules that undergo a significant change in shape between their high- and low-spin states with aromatic donor groups that interdigitate in the crystal lattice.⁵ Both factors lead to efficient mechanical coupling between molecular switching centers, thus propagating the transition through the crystal more effectively. We are testing this hypothesis with new complexes designed to obey these criteria,¹⁰ which has inspired the following study.

The compounds $[\text{Fe}(\text{H}_2\text{Bpz}_2)_2(\text{L})]$ (L = 2,2-bipyridine [bipy], 1; L = 1,10-phenanthroline [phen], 2; Chart 1) were first prepared by Real et al. over 15 years ago.¹¹ They are isostructural at room temperature, and both undergo SCO near 160 K. However, while 2 exhibits an abrupt spin transition with a narrow hysteresis loop, 1 undergoes a more gradual spin equilibrium centered at the same temperature.^{11,12} This reflects a crystallographic phase change between the spin states that is exhibited by 2 but not by 1.¹³ More recently, vacuum deposition of 2 onto Au(111) or other surfaces has led to the observation of SCO in nanometer thin films,^{14–17} and the imaging of individual molecules in different spin states.¹⁴ Other groups have also prepared SCO-active derivatives of 1 and 2, containing bipyridyl ligands with radical or photoactive pendant groups.¹⁸ We describe here four new analogues of 1 and 2 containing annelated bipyridyl ligands, $[\text{Fe}(\text{H}_2\text{Bpz}_2)_2(\text{L})]$ (L = dipyrido[3,2-*f*:2',3'-*h*]-quinoxaline [dpq], 3; L = dipyrido[3,2-*a*:2'3'-*c*]phenazine [dppz], 4; L = dipyrido[3,2-*a*:2'3'-*c*]benzo[*i*]phenazine [dppn], 5; L = dipyrido[3,2-*a*:2',3'-*c*](6,7,8,9-tetrahydro)phenazine [dppc], 6). Molecules in 3–6 have potential to interdigitate in the solid state via their extended aromatic bipyridyl substituents, so they are a promising testbed to determine the effect of that interdigitation on SCO behavior.

Received: June 13, 2014

Published: August 29, 2014

Chart 1. Compounds Referred to in This Work



EXPERIMENTAL SECTION

Unless otherwise stated, all reactions were carried out in air using as-supplied analytical reagent-grade solvents. Potassium dihydrido-bispyrazolylborate ($K[H_2Bpz_2]$)¹⁹ and the bipyridyl heterocycles dpq,²⁰ dpz,²¹ dppc,²⁰ and dppn²² were prepared by the literature procedures. Other reagents and solvents were purchased commercially and used as supplied.

Synthesis of $[Fe(H_2Bpz_2)_2(dpq)]$ (3). To a solution of $K[H_2B(Pz)_2]$ (0.16 g, 0.88 mmol) in methanol (10 cm³) was added a solution of $Fe[ClO_4]_2 \cdot 6H_2O$ (0.16 g, 0.44 mmol) in methanol (5 cm³). The $KClO_4$ precipitate was removed by filtration, affording a yellow solution. A solution of dpq (0.10 g, 0.44 mmol) in a 1:1 v/v methanol/chloroform mixture (10 cm³) was then added dropwise, causing an

immediate color change to dark violet. After the solution was stirred for 30 min at room temperature the violet precipitate was collected, washed with methanol, and dried under a stream of N_2 . Yield 0.11 g, 38%. Slow diffusion of diethyl ether into a dichloromethane solution of this crude product afforded a mixture of two crystal phases, namely, 3-2dpq (blocks) and 3-0.5dpq (needles), which were both crystallographically characterized. Elemental analysis of the bulk material was consistent with a formulation of 3-*ndpq* with $n \approx 1$, implying it contains a mixture of both phases. That was subsequently confirmed by X-ray powder diffraction. Elemental analysis for $C_{26}H_{24}B_2FeN_{12} \cdot C_{14}H_8N_4$ found, (calcd) (%): C 58.7 (59.0), H 4.00 (3.96), N 27.1 (27.5). Slow diffusion of *n*-hexane into a toluene solution of 3 afforded a homogeneous sample of 3-2C₇H₈. Most of the toluene was retained upon exposure of the crystals to air. Elemental analysis for $C_{26}H_{24}B_2FeN_{12} \cdot 1.5C_7H_8$ found, (calcd) (%): C 61.1 (60.8), H 5.10 (5.04), N 23.0 (23.3).

Synthesis of $[Fe(H_2Bpz_2)_2(dppz)]$ (4). Method as for 3, using dppz (0.12 g, 0.44 mmol), which yielded a violet precipitate of 4. Yield 0.15 g, 65%. Recrystallization from dichloromethane/pentane afforded a mixture of products, including crystals of uncoordinated dppz, which are described in the Supporting Information, and a powder whose microanalysis was consistent with the monohydrate of the complex. Elemental analysis for $C_{30}H_{26}B_2FeN_{12} \cdot H_2O$ found, (calcd) (%): C 55.5 (55.4), H 4.00 (4.34), N 26.1 (25.8). The solvate crystals 4-1.5C₇H₈ were grown by slow diffusion of *n*-hexane into a toluene solution of the crude complex. Elemental analysis for $C_{30}H_{26}B_2FeN_{12} \cdot C_7H_8 \cdot 1.5H_2O$ found, (calcd) (%): C 59.1 (59.2), H 4.50 (4.96), N 21.9 (22.4).

Synthesis of $[Fe(H_2Bpz_2)_2(dppn)]$ (5). Method as for 3, using dppn (0.15 g, 0.44 mmol). The crude product was isolated as a brown precipitate. Yield 0.13 g, 59%. Slow diffusion of hexanes into a toluene solution of 5 afforded crystals of formula 5-1.5C₇H₈·0.5C₆H₁₄, which retain 1 equiv of toluene upon exposure to air. Elemental analysis for $C_{34}H_{28}B_2FeN_{12} \cdot C_7H_8 \cdot 0.5H_2O$ found, (calcd) (%): C 62.9 (62.8), H 4.80 (4.76), N 21.1 (21.4). Dark brown crystals of 5 were obtained by layering a freshly prepared methanolic solution of $Fe[H_2B(Pz)_2]_2$ above a solution of dppn in 1,2-dichloroethane. The crystals are solvent-free according to X-ray diffraction, but absorb atmospheric moisture by microanalysis. Elemental analysis for $C_{34}H_{28}B_2FeN_{12}$

Table 1. Experimental Details for the Lowest Temperature Structure Determination of Each Compound in This Study. Comparable Data at Other Temperatures, Where They Were Measured, Are Given in the Supporting Information

	3-2dpq	3-0.5dpq	3-2C ₇ H ₈	4-1.5C ₇ H ₈	5-1.5C ₇ H ₈ ·0.5C ₆ H ₁₄	5	6·(C ₃ H ₇) ₂ O
<i>T</i> /K	100(2)	100(2)	120(2)	100(2)	100(2)	100(2)	100(2)
formula	C ₅₄ H ₄₀ B ₂ FeN ₂₀	C ₃₃ H ₂₈ B ₂ FeN ₁₄	C ₄₀ H ₄₀ B ₂ FeN ₁₂	C _{40.5} H ₃₈ B ₂ FeN ₁₂	C _{47.5} H ₄₇ B ₂ FeN ₁₂	C ₃₄ H ₂₈ B ₂ FeN ₁₂	C ₃₆ H ₄₄ B ₂ FeN ₁₂ O
fw	1046.53	698.16	766.31	770.30	863.44	682.15	738.30
cryst syst	monoclinic	triclinic	monoclinic	triclinic	triclinic	triclinic	tetragonal
space group	C2/c	$P\bar{1}$	C2/c	$P\bar{1}$	$P\bar{1}$	$P\bar{1}$	$I4_1/acd$
<i>a</i> /Å	26.1535(13)	10.6128(5)	13.610(3)	10.0737(6)	12.3397(6)	9.2401(6)	33.5926(7)
<i>b</i> /Å	13.8310(6)	16.4464(10)	22.354(5)	11.2795(7)	12.9186(5)	11.2022(8)	
<i>c</i> /Å	14.9300(7)	18.9257(12)	13.472(4)	16.3872(14)	15.3077(7)	16.0929(10)	14.4627(4)
α /deg		84.728(5)		83.496(6)	70.730(4)	75.937(6)	
β /deg	119.592(3)	87.421(5)	111.87(3)	87.140(6)	72.279(4)	82.685(5)	
γ /deg		74.223(5)		87.963(5)	85.753(3)	87.501(5)	
<i>V</i> /Å ³	4696.2(4)	3164.8(3)	3803.8(17)	1846.9(2)	2193.26(17)	1602.55(18)	16320.6(7)
<i>Z</i>	4	4	4	2	2	2	16
<i>D</i> _{calcd} /g cm ⁻³	1.480	1.465	1.338	1.385	1.307	1.414	1.202
reflns collected	13446	24269	7815	11808	23388	11181	14932
unique reflns	5649	14597	3341	6467	10449	5448	3634
<i>R</i> _{int}	0.057	0.062	0.102	0.053	0.045	0.050	0.049
<i>R</i> ₁ , <i>I</i> > 2σ(<i>I</i>) ^a	0.062	0.079	0.103	0.063	0.062	0.046	0.085
<i>wR</i> ₂ , all data ^b	0.158	0.172	0.294	0.153	0.159	0.109	0.285
GOF	1.049	1.038	1.061	1.067	1.047	1.022	1.076

$$^a R = \sum [|F_o| - |F_c|] / \sum |F_o| \quad ^b wR = [\sum w(F_o^2 - F_c^2) / \sum wF_o^4]^{1/2}$$

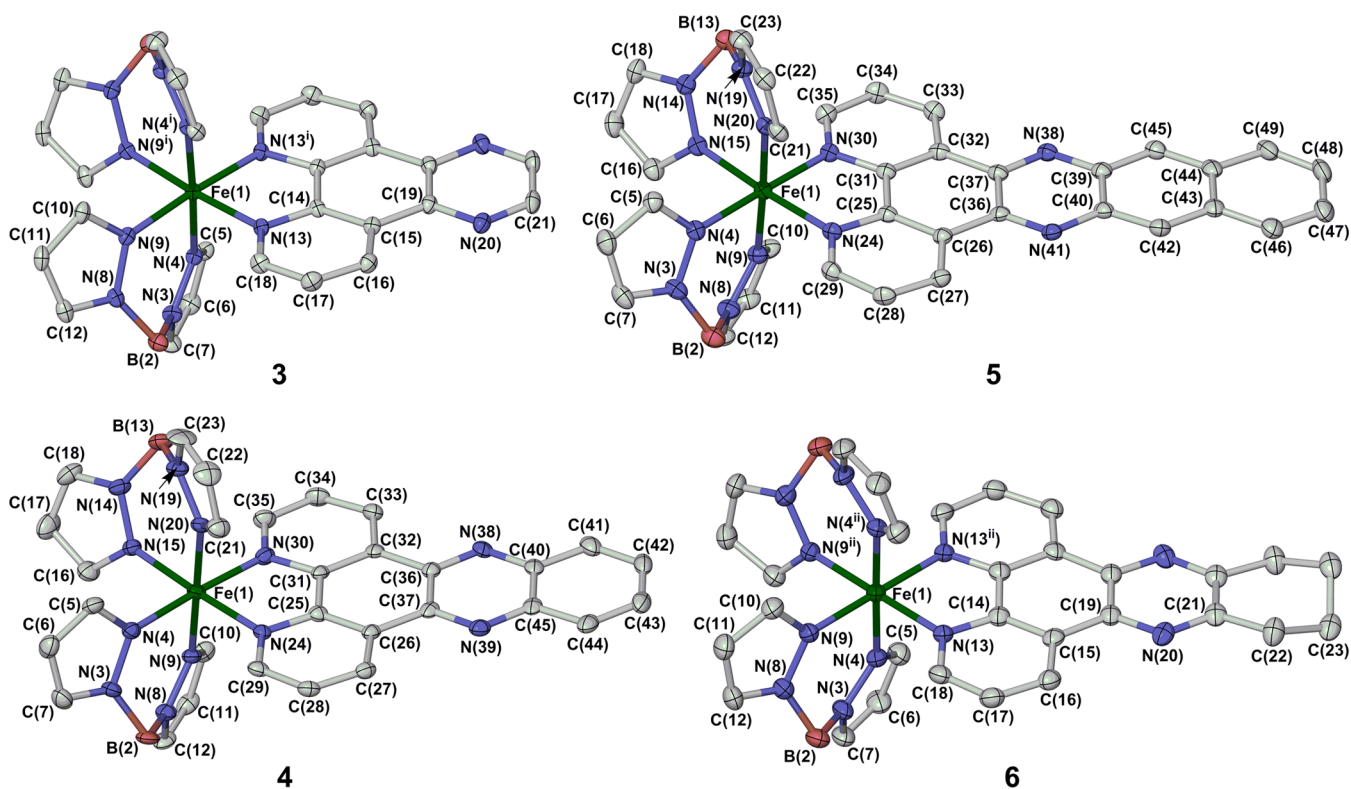


Figure 1. Views of the complex molecules in the crystal structures of **3**·2dpq, **4**·1.5C₇H₈, **5**·1.5C₇H₈·0.5C₆H₁₄ and **6**·(C₃H₇)₂O at 100 K. Atomic displacement ellipsoids are drawn at the 50% probability level, and H atoms have been omitted. Symmetry codes: (i) $-x, y, 1/2-z$; (ii) $x, 1-y, 3/2-z$. Color code: C, white; B, pink; Fe, green; N, blue.

0.5H₂O found, (calcd) (%): C 58.7 (59.1), H 4.05 (4.23), N 24.0 (24.3).

Synthesis of [Fe(H₂Bpz₂)₂(dppc)] (6**).** Method as for **3**, using dppc (0.13 g, 0.44 mmol), which gave **6** as a violet precipitate. Yield 0.11 g, 49%. Diffusion of di-isopropyl ether into a solution of **6** in chloroform afforded crystals of formula **6**·(C₃H₇)₂O according to a crystallographic analysis, although some of the solvent is apparently replaced by atmospheric moisture upon exposure to air. Elemental analysis for C₃₀H₃₀B₂FeN₁₂·0.5C₆H₁₄O·H₂O found, (calcd) (%): C 56.6 (56.2), H 5.60 (5.57), N 23.6 (23.8). Slow diffusion of hexanes into a toluene solution of **6** afforded needlelike crystals that were not suitable for X-ray analysis. Microanalysis and thermogravimetric analysis (TGA) data imply these crystals contain toluene, most of which is lost upon exposure to air. Elemental analysis for C₃₀H₃₀B₂FeN₁₂·0.25C₇H₈·0.33H₂O found, (calcd) (%): C 56.9 (57.3), H 4.70 (4.95), N 25.7 (25.3).

Single-Crystal X-ray Structure Determinations. All diffraction data were collected with an Agilent Supernova dual-source diffractometer using monochromated Mo K α radiation ($\lambda = 0.71073$ Å), except for **5** and **6**·(C₃H₇)₂O where monochromated Cu K α radiation ($\lambda = 1.54184$ Å) was employed. Experimental details of structure determinations of each compound at 100 K are given in Table 1. Comparable data at other temperatures are available in the Supporting Information. All the variable-temperature crystallographic studies employed the same crystal of each complex at all temperatures. The structures were solved by direct methods (SHELXS97²³) and were developed by full least-squares refinement on F^2 (SHELXL97²³). Crystallographic figures were prepared using X-SEED,²⁴ which incorporates POVray,²⁵ and coordination volumes (V_{Oh}) were calculated using Olex2.²⁶ Additional crystallographic information is available in the Supporting Information.

X-ray Structure Refinements. Unless otherwise stated, all fully occupied non-H atoms were refined anisotropically, and H atoms were placed in calculated positions and refined using a riding model.

The asymmetric unit of **3**·2dpq contains half a molecule of the complex, with Fe(1) lying on a 2-fold rotation axis, and a whole molecule of dpq in a general crystallographic position. A full variable temperature study of this crystal between 100 and 300 K was carried out. In contrast, the asymmetric unit of **3**·0.5dpq contains two unique molecules of the complex and one molecule of dpq, all on general crystallographic positions. This structure was only determined at 100 K, since it remains in the high-spin state at that temperature. Crystals of **3**·2C₇H₈ are poor diffractors of X-rays, possibly because of their needle morphology. While data sets at several temperatures were collected, only the best refinement is reported here ($T = 120$ K). The asymmetric unit contains half a complex molecule, with Fe(1) lying on the C₂ axis $1/2, y, 1/4$; and, two half-molecules of toluene spanning the crystallographic inversion centers $1/2, 1, 1/2$ and $1/2, 1/2, 1/2$.

Full structural refinements for **4**·1.5C₇H₈ were obtained between 100 and 240 K, at 20 K intervals. Its asymmetric unit contains one molecule of the complex, one molecule of toluene, and a second half molecule of toluene spanning the inversion center at the origin. No disorder was incorporated in the model for any of these refinements, although high displacement ellipsoids on the solvent half-molecule imply that unresolved dynamic disorder may be present in that residue above 180 K. The asymmetric unit of solvent-free **5** simply contains a molecule of the complex on a general crystallographic site. Useful X-ray analyses of **5**·1.5C₇H₈·0.5C₆H₁₄ were achieved at 100, 120, 140, 160, and 180 K, although the refinements above 140 K are of lower quality owing to increased solvent disorder. The asymmetric unit contains: one molecule of the complex; a half-molecule of toluene located on the inversion center $1/2, 0, 0$, which is crystallographically ordered at all temperatures; a half-occupied, complete molecule of toluene near the inversion center $1/2, 0, 1/2$, which becomes disordered above 140 K; and, a disordered region of solvent on a general crystallographic site which was modeled using half-molecules of toluene and hexane disordered over the same position.

Crystals of **6**·(C₃H₇)₂O were weakly diffracting, and a refinement could only be achieved at 100 K. The asymmetric unit contains half a

complex molecule, with Fe(1) lying on a 2-fold rotation axis. There are also square channels of ca. $8.3 \times 8.3 \text{ \AA}$ running parallel to (001), of volume 5736.3 \AA^3 per unit cell which is 35.1% of the total cell volume. The contents of the pores could not be resolved, but a *SQUEEZE* analysis²⁷ demonstrated the pore contents correspond to 731 electrons per asymmetric unit, or 45.7 electrons per complex molecule. That could correspond to 0.8 equiv of chloroform (59 electrons per molecule) or di-isopropyl ether (58 electrons per molecule), the two solvents used to grow these crystals. Since the microanalysis was more consistent with the presence of di-isopropyl ether, one equiv of that solvent was added to the formula for the density and $F(000)$ calculations.

Other measurements. Magnetic susceptibility measurements were performed with freshly isolated, unground polycrystalline samples, using a Quantum Design SQUID/VSM magnetometer in an applied field of 5000 G and a temperature ramp of 5 K min^{-1} . Diamagnetic corrections for the samples were estimated from Pascal's constants;²⁸ a previously measured diamagnetic correction for the sample holder was also applied to the data. The same samples were then recovered and used for the thermogravimetric analyses, which employed a TA Instruments TGA Q50 analyzer with a temperature ramp of 10 K min^{-1} under a stream of nitrogen gas. Hence the TGA analyses should accurately reflect the compositions of the samples used for the magnetic susceptibility measurements. Elemental microanalyses were performed by the University of Leeds School of Chemistry microanalytical service, again using the same samples of the compounds. The samples were exposed to air for longer during the microanalysis determinations than for the TGA measurements, which may account for discrepancies between the solvent content implied by the two techniques. X-ray powder diffraction patterns were measured from ground polycrystalline samples, using a Bruker D2 Phaser diffractometer.

RESULTS

Following the method reported for **1** and **2**,¹¹ hydrated $\text{Fe}[\text{ClO}_4]_2$ was treated with 2 equiv $\text{K}[\text{H}_2\text{Bpz}_2]$ ¹⁹ and 1 equiv of the appropriate bipyridyl chelate^{20–22} in a methanol/chloroform solvent mixture. Initial attempts to crystallize the complexes from chlorinated solvents gave mixed results. Solvent-free crystals of **5** and a solvate of **6** were cleanly obtained in this way, but **3** afforded a mixture of two phases **3·2dpq** and **3·0.5dpq**, both containing uncomplexed dpq ligand in addition to the target iron complex. Compound **4** also yielded a mixture of compounds from chlorinated solvents, including the metal-free dppz ligand (Supporting Information). Hence, the complexes appear to undergo ligand redistribution reactions, even in weakly associating chlorinated solvents. Crystallizations from toluene/hexane mixtures proceeded more cleanly, yielding homogeneous samples of crystallographic composition **3·2C₇H₈**, **4·1.5C₇H₈** and **5·1.5C₇H₈·0.5C₆H₁₄**. Attempts to obtain a comparable toluene solvate of **2** yielded only the previously published unsolvated crystal form.^{11,13}

All these crystals contain the expected six-coordinate complex molecules (Figure 1). Their metric parameters imply the complexes are low-spin at the lowest temperature measured (100 or 120 K) except for **3·0.5dpq** and unsolvated **5**, which are both high-spin at 100 K. Variable temperature crystallographic studies of **3·2dpq** and **4·1.5C₇H₈** demonstrated that both compounds undergo gradual SCO on warming (Figure 2 and the Supporting Information). The crossover occurs between ca. 100 and 200 K in single crystals of **3·2dpq**, while for **4·1.5C₇H₈** the transition begins around 160 K but is still incomplete at 240 K, the highest temperature where diffraction quality was sufficient for a full structural analysis. A similar experiment for **5·1.5C₇H₈·0.5C₆H₁₄** only gave useful diffraction data at $T \leq 180 \text{ K}$, the apparent onset of SCO in that compound.

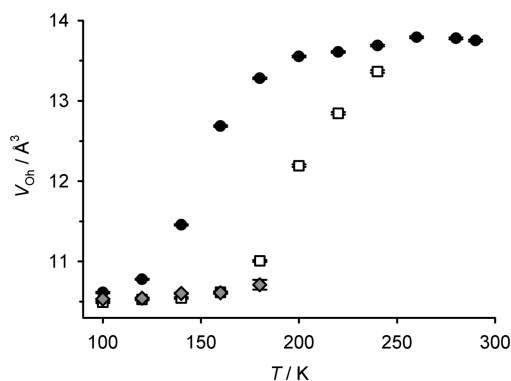


Figure 2. Variation in spin-state with temperature from the volume of the FeN_6 octahedron in **3·2dpq** (●), **4·1.5C₇H₈** (□), and **5·1.5C₇H₈·0.5C₆H₁₄** (shaded gray diamond). Error bars are smaller than the symbols on the graph. These, and other crystallographic data, are tabulated in the Supporting Information.

These transitions are most easily monitored by following the volume of the coordination octahedron (V_{Oh}) around the iron center as a function of temperature, which is ca. 10.5 \AA^3 in the low-spin state and 13.5 \AA^3 in the high-spin state for compounds of this type.¹³ The alternative, angular distortion indices Σ and Θ that are often used to monitor crystallographic spin-states²⁹ are less useful for **1–6**, because the six-membered chelate rings formed by the $[\text{H}_2\text{Bpz}_2]^-$ ligands afford *cis*-N–Fe–N angles close to the ideal value of 90° in both spin states.⁵ The variation in V_{Oh} with temperature in **3·2dpq** and **4·1.5C₇H₈** (Figure 2) closely mirrors the thermal dependence of the spin-equilibrium in bulk samples of those materials, as determined from magnetic susceptibility data (Supporting Information).

All the crystalline phases contain the expected stacks of interdigitated molecules, which interact through intermolecular face-to-face π – π interactions between the annelated bipyridyl ligands; and, in some cases, by C–H \cdots π contacts from the bipyridyl ligand to a pyrazolyl group in a neighboring molecule. All of the crystal structures except one (see below) contain one-dimensional (1D) molecular stacks generated by crystallographic inversion symmetry, although the composition and topology of the stacks varies between compounds (Figures 3 and 4, and the Supporting Information). All the toluene solvates contain toluene molecules sandwiched between complex molecules in the stacks, in an ABABAB (**3·2C₇H₈**) or AABAAB (**4·1.5C₇H₈** and **5·1.5C₇H₈·0.5C₆H₁₄**; A = complex, B = toluene) arrangement. These toluene sites are all disordered about crystallographic inversion centers, and become significantly more disordered as the temperature is raised. The molecular stacking in unsolvated **5** is similar to its solvate, but with every other molecule displaced horizontally (to the left in Figure 4) by ca. 11 \AA , filling the space left by the absent toluene guest. The interplanar distances between adjacent bipyridyl ligands in the stacks range from 3.35 to 3.49 \AA at 100 K, which are typical values for π – π interactions between two identical arenes.³⁰ The distances between bipyridyl and toluene nearest neighbors are harder to quantify because of the solvent disorder, but are slightly longer at 3.5 – 3.7 \AA . The horizontal offset in these stacks increases in the order **3·2C₇H₈** < **4·1.5C₇H₈** < **5·1.5C₇H₈·0.5C₆H₁₄** < **5**, following the length of the heterocyclic ligands.

All three toluene solvates also contain channels of solvent, either toluene or a toluene/hexane mix, running parallel to the molecular stacks (Figure 5 and the Supporting Information).

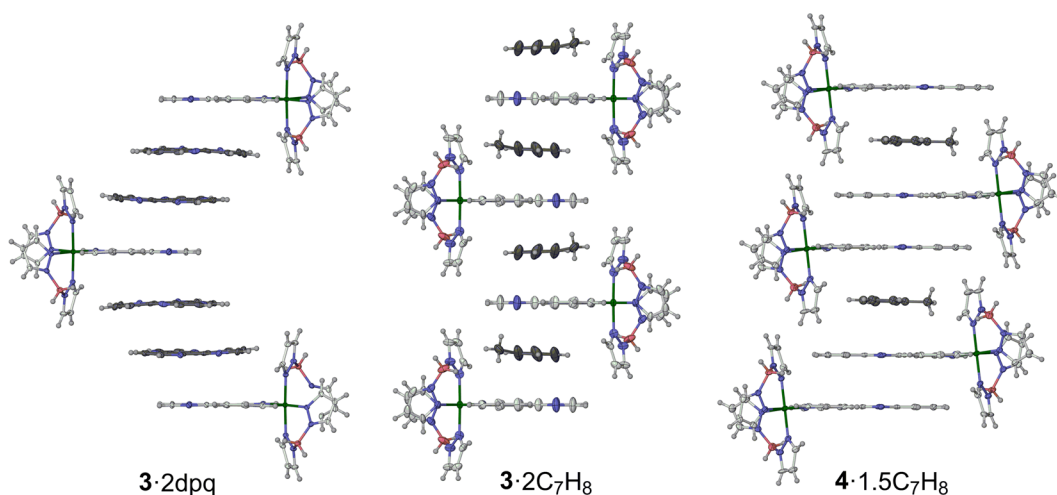


Figure 3. 1D stacking motifs in the structures of solvated **3** and **4**. Atomic displacement ellipsoids are drawn at the 50% probability level except for H atoms which have arbitrary radii, and only one orientation of the disordered toluene sites is shown. Color code: C{complex}, white; C{dpq or toluene}, dark gray; H, pale gray; B, pink; Fe, green; N, blue.

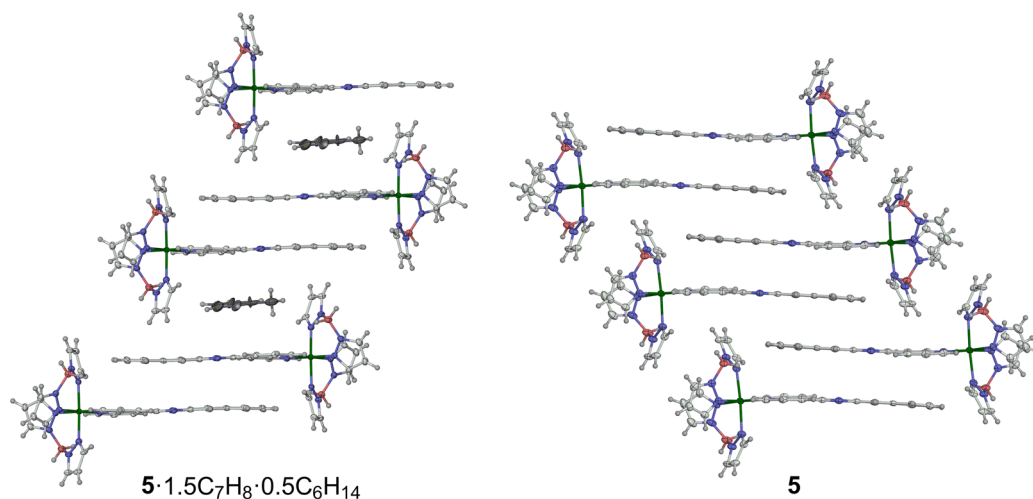


Figure 4. 1D stacking motifs in solvated and unsolvated **5**. The views are chosen to emphasize the relationship between the two structures. Other details as for Figure 3

Although reasonably ordered at 100 K, the channel contents become disordered as the temperature is raised. The increased disorder in the in-stack and in-channel solvent accounts for the lower quality of diffraction from these crystals at higher temperatures. The walls of the channels are formed predominantly from the pyrazolylborate ligands, implying that those are in less rigid, more open lattice environments than the bipyridyl ligands in the molecular stacks. That is important to the following discussion of the spin state properties of the compounds.

The 3/dpq cocrystals also contain 1D molecular stacks. The stacks in 3·2dpq have an ACCACC (A = complex, C = dpq) composition, yielding S-shaped stacks undulating along the crystallographic $[101]$ vector (Figure 3). In contrast, 3·0.5dpq contains linear stacks with an AACAAC arrangement. Intra-stack C–H $\cdots\pi$ contacts between the free dpq, and pyrazolyl groups on the adjacent complex molecules, cause significant distortions to the structure of the complex which may account for the stabilization of the high-spin state in this material down to 100 K (Supporting Information).

The exception to the above discussion is $6\cdot(\text{C}_3\text{H}_7)_2\text{O}$, whose complex molecules are stacked about a crystallographic 4_1 axis. Adjacent, overlapping dpqc ligands are separated by 3.587(19) Å, implying only a weak π – π interaction between them.³⁰ The stacks form the corners of square pores running parallel to the c axis, of approximate dimensions 8.3×8.3 Å (Figure 6). The pores are filled with ca. 1 mol equiv of disordered solvent according to SQUEEZE,²⁷ which is probably di-isopropyl ether from microanalysis of the bulk material.

Elemental microanalysis and TGA measurements were performed on the same samples used for the magnetic measurements described below. These analytical data from the toluene solvates imply that a fraction of their lattice solvent is readily lost or replaced by lattice water, which presumably corresponds to the contents of the channels in the crystal lattices. Between 0.75 and 1.5 equiv of toluene are retained by the solvates of 3–5 under ambient conditions, however. Hence the less accessible toluene molecules within the molecular stacks appear to remain in the materials upon exposure to air, so the stacked structures may retain their integrity. Bulk samples of the free ligand cocrystallate 3·ndpq analyze

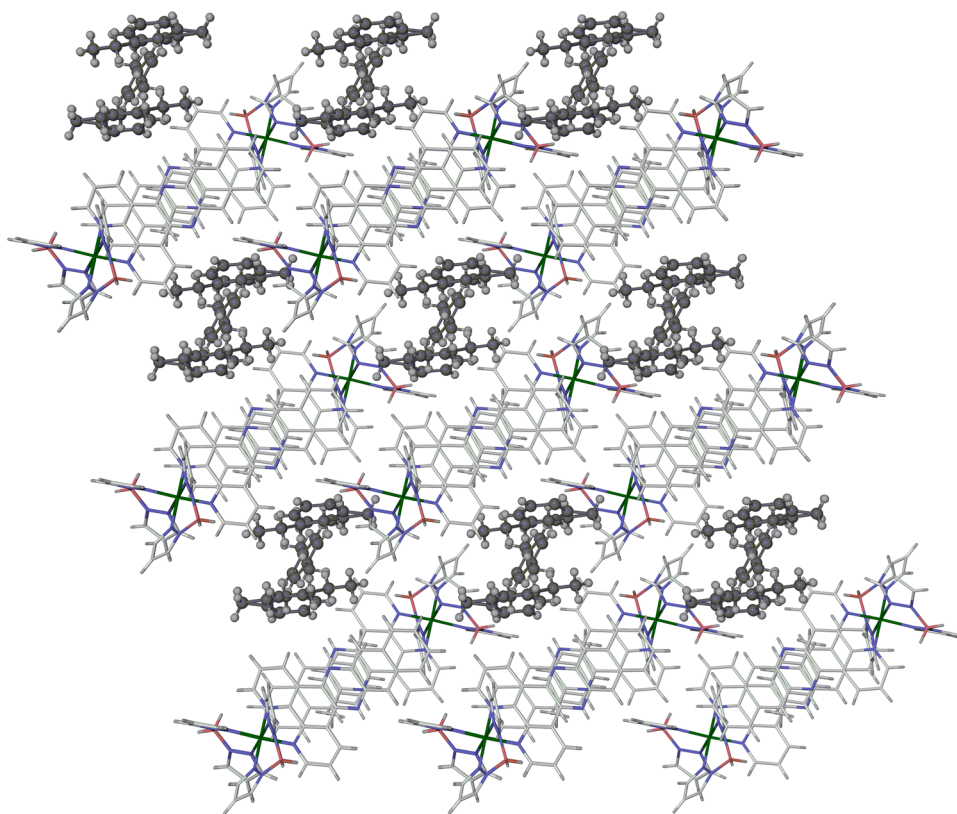


Figure 5. Packing diagram of $5 \cdot 1.5\text{C}_7\text{H}_8 \cdot 0.5\text{C}_6\text{H}_{14}$, showing the channels containing a disordered mixture of toluene and pentane. All atoms have arbitrary radii, with the complex molecules being de-emphasized. The view is along the $[100]$ vector. Color code: C{stacks}, white; C{channel solvent}, dark gray; H, pale gray; B, pink; Fe, green; N, blue.

consistently with $n \approx 1$, implying that they contain a mixture of both $3 \cdot 2\text{dpq}$ and $3 \cdot 0.5\text{dpq}$. That suggestion was supported by X-ray powder diffraction, and is also consistent with the magnetic susceptibility data described below.

It is clear from magnetic susceptibility measurements that all the compounds are high-spin at room temperature and exhibit rather gradual SCO equilibria on cooling (Figure 7). Spin-crossover in $3 \cdot 1.5\text{C}_7\text{H}_8$ proceeds to completion, with a midpoint temperature ($T_{1/2}$) of 147 K. The susceptibility data for $3 \cdot \text{ndpq}$ are virtually identical to the toluene solvate above 120 K, but show a residual high-spin iron population at lower temperatures, which can be attributed to the fraction of the sample adopting the high-spin $3 \cdot 0.5\text{dpq}$ phase. The spin-equilibria in the toluene solvates of **4** and **5** are also very similar, with $T_{1/2}$ values of 188 ± 1 K. Interestingly, a small thermal hysteresis loop between $165 \leq T \leq 185$ K is apparent in the transition for $5 \cdot \text{C}_7\text{H}_8 \cdot 0.5\text{H}_2\text{O}$, which is not shown by $4 \cdot x\text{C}_7\text{H}_8$. A possible structural origin for this hysteresis is discussed below. The toluene-free sample $5 \cdot 0.5\text{H}_2\text{O}$ also exhibits the onset of SCO below 150 K, but ca. 75% of the sample becomes thermally trapped in its high-spin state below 70 K. Since X-ray powder diffraction confirmed that the sample was phase-pure, this is likely to reflect kinetic trapping of the majority of the iron centers in their high-spin state below their high \rightarrow low spin relaxation temperature. Such thermal trapping of a residual, metastable high-spin fraction³¹ is commonly found in spin-transitions extending below 100 K.³² The compound is still 85% high-spin at 100 K according to this technique, which is consistent with the high-spin nature of the unsolvated crystals of **5** at that temperature. Lastly, the solvate phases of **6** exhibit gradual SCO with $T_{1/2} = 133$ K ($6 \cdot 0.25\text{C}_7\text{H}_8 \cdot 0.5\text{H}_2\text{O}$) and 181

K ($6 \cdot 0.5\text{C}_6\text{H}_{14} \cdot \text{O} \cdot \text{H}_2\text{O}$), both with a 15–20% frozen-in high-spin residue below 70 K (Figure 7).

DISCUSSION

Complexes **3–6** all adopt crystal structures based on 1D stacking of their annelated bipyridyl ligands, as predicted at the beginning of this study, although in many cases these stacks contain intercalated toluene or free dpq ligand as well as the complex molecule. However, all the compounds exhibit gradual SCO transitions despite the strong interactions between the switching centers that should arise from this interdigitation. Some insight is provided by comparison of the high- and low-spin crystal structures of $3 \cdot 2\text{dpq}$ and $4 \cdot 1.5\text{C}_7\text{H}_8$. In both cases, the intermolecular dimensions within the stacks do not change significantly during the spin transition (tabulated in the Supporting Information). Rather, most of the structural rearrangement accompanying SCO involves the $[\text{Fe}(\text{H}_2\text{Bpz}_2)_2]$ fragments, which expand into the less densely packed space between the stacks (Figure 8). This includes a displacement of the iron atoms away from the center of the stacks in the high-spin state, reflecting a lengthening of the Fe–N bonds to the bipyridyl chelates by 0.23–0.24 Å. Hence, the structural changes during SCO are taking place predominantly in the least rigid regions of the lattice; that is, between the stacks rather than within them. That explains why different molecular stacking motifs have no apparent influence on SCO in these materials.

The magnetic susceptibility data from $5 \cdot \text{C}_7\text{H}_8 \cdot 0.5\text{H}_2\text{O}$ show an unusual, narrow thermal hysteresis at the low-spin side of its SCO transition (Figure 7). A possible explanation for this is provided by the crystalline solvate $5 \cdot 1.5\text{C}_7\text{H}_8 \cdot 0.5\text{C}_6\text{H}_{14}$, which

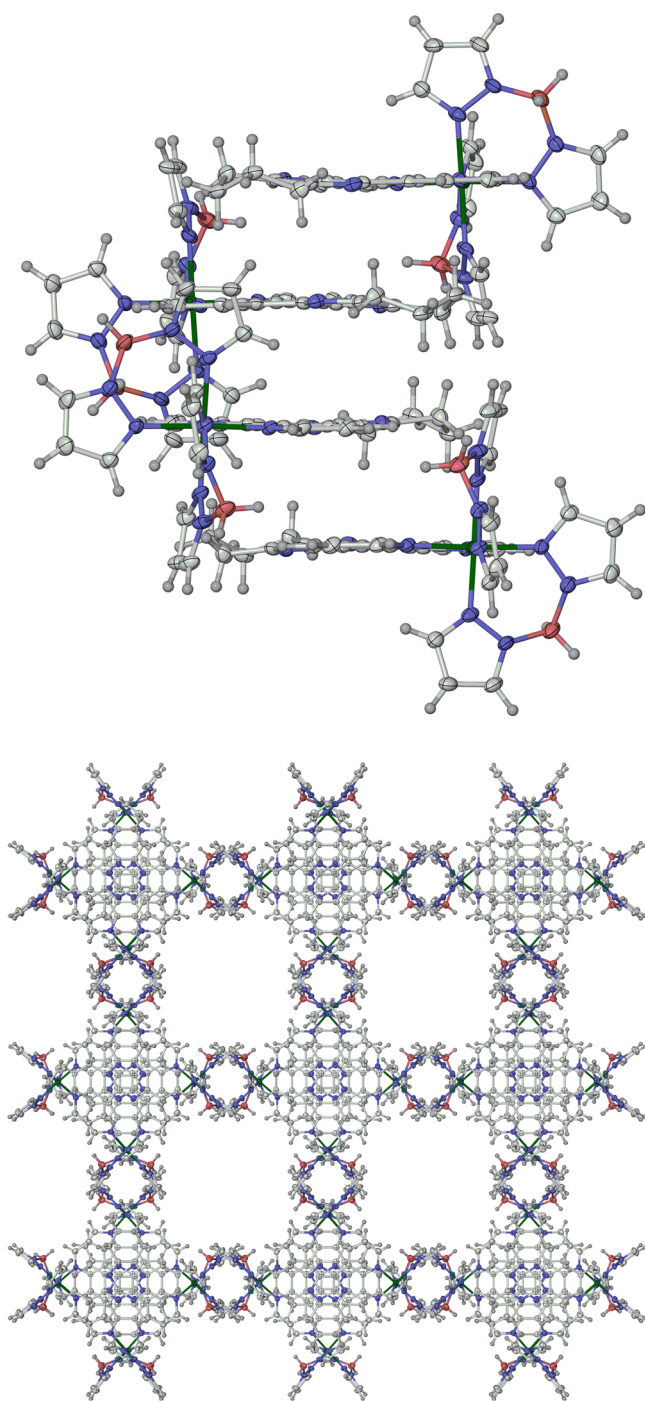


Figure 6. (top) View of a molecular stack in $6 \cdot (\text{C}_3\text{H}_7)_2\text{O}$, formed by a crystallographic 4_1 screw axis. (lower) Packing diagram perpendicular to the crystallographic (001) plane, showing the channels in the lattice. Other details as for Figure 5.

undergoes a significant structural rearrangement within the stacks between 140 and 180 K (Figure 9). This rearrangement is not coupled to SCO, since the crystalline complex is low-spin at all these temperatures. Rather, it involves a displacement of Fe(1) by 0.28 Å along the direction of the stacks, accompanied by a change in conformation in the dppn ligand from an S-shape at 100 K to a more planar structure at 180 K. This widens the toluene-binding pocket in the stacks by 0.282(7) Å, leading to substantially increased disorder in the toluene molecule at the higher temperatures. We attribute this behavior to a

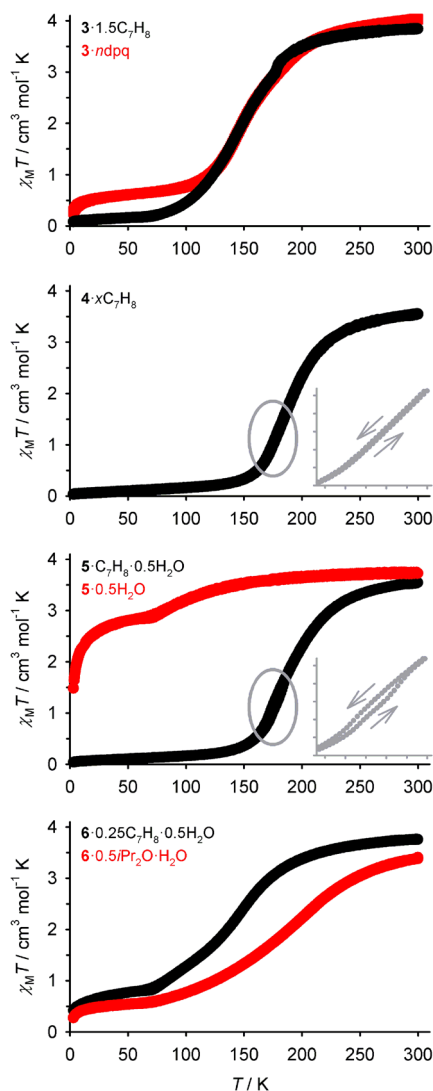


Figure 7. Variable-temperature magnetic susceptibility data for the toluene solvate phases (black) and the toluene-free materials (red) of 3–6. The insets show the absence and presence of thermal hysteresis for the toluene solvates of 4 and 5, respectively.

symmetry-related pair of C–H $\cdots\pi$ contacts spanning the toluene binding pocket, which are positioned to impose the S-shaped ligand conformation on the low-temperature structure (Figure 9). This geometry of C–H $\cdots\pi$ interaction is only present in $5 \cdot 1.5\text{C}_7\text{H}_8 \cdot 0.5\text{C}_6\text{H}_{14}$, because of the extra length of the dppn ligand compared to dpq in 3 or dppz in 4 (Figures 3 and 4), and a similar structural rearrangement could give rise to the SCO hysteresis in the bulk material derived from this crystal phase. The stabilization of the high-spin state in toluene-free 5 is harder to explain but may relate to the absence of solvent channels between the molecular stacks in that material, leading to a more crowded environment about the [Fe-(H₂Bpz₂)₂] fragment.

CONCLUSION

This work has improved our understanding of the crystal engineering of cooperative SCO materials with interdigitated switching centers.^{5,10} It has shown that interdigitation of SCO molecules is not enough, on its own, to engineer a cooperative spin-transition into a molecular material if other regions of the

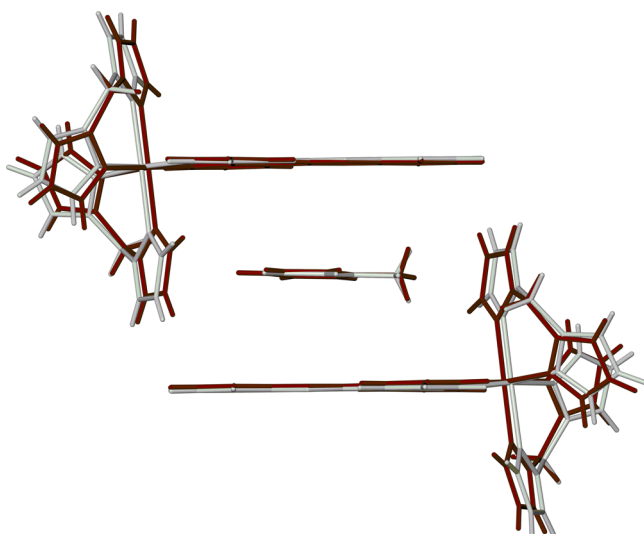


Figure 8. Overlay of the $[C_7H_8C(4)_2]$ assembly in $4 \cdot 1.5C_7H_8$ at 100 K (low-spin, red) and 240 K (predominantly high-spin, white). Only one orientation of the disordered toluene molecule is shown.

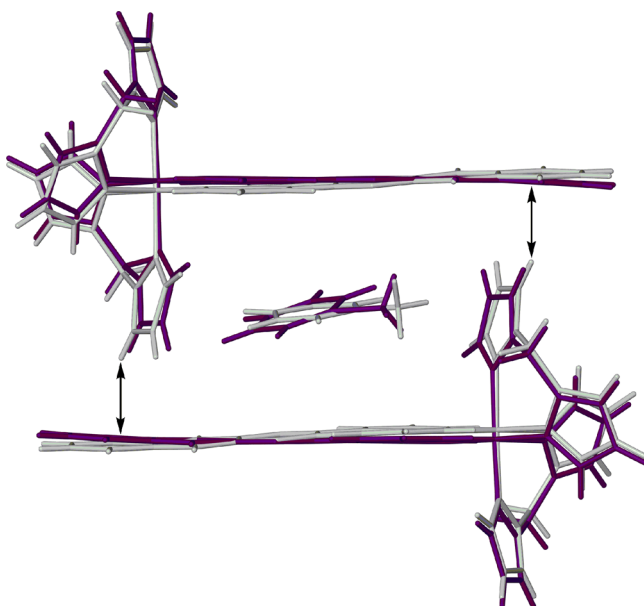


Figure 9. Overlay of the $[C_7H_8C(5)_2]$ assembly in $5 \cdot 1.5C_7H_8 \cdot 0.5C_6H_{14}$ at 100 K (white) and 180 K (purple). The compound is low-spin at both temperatures. Only one orientation of the disordered toluene molecule is shown. The arrows show the intermolecular C–H... π contacts that may be responsible for this structural rearrangement.

crystal are less densely packed (such as channels of disordered solvent). In that case the structural changes during SCO may occur preferentially in the less rigid regions of the lattice, so any cooperativity promoted by strong interactions between interlocked nearest neighbor molecules is lost. Our current work aims to build on these results, to produce new cooperative SCO crystals by a bottom-up approach.

■ ASSOCIATED CONTENT

📄 Supporting Information

Additional crystallographic data; illustrations of data to compare spin-crossover transition, to view molecular stacks,

to view overlay of structures, to view asymmetric structural unit, and to view packing diagrams. Tabulated data indicating $\pi \cdots \pi$ interaction and hydrogen bonds, additional experimental details, selected bond lengths and angles; TGA and X-ray powder diffraction measurements; crystallographic information files (CIF). This material is available free of charge via the Internet at <http://pubs.acs.org>. CCDC 1007558–1007568 (3·2dpq), 1007569 (3·0.5dpq), 1007570 (3·2C₇H₈), 1007571–1007578 (4·1.5C₇H₈), 1007579–1007583 (5·1.5C₇H₈·0.5C₆H₁₄), 1007584 (5), 1007585 (6·(C₃H₇)₂O), and 1007586 (dppz·CHCl₃) contain the supplementary crystallographic data for this Paper. These data can be obtained free of charge from the Cambridge Crystallographic Data Center via www.ccdc.cam.ac.uk/data_request/cif.

■ AUTHOR INFORMATION

Corresponding Author

*E-mail: m.a.halcrow@leeds.ac.uk

Notes

The authors declare no competing financial interest.

■ ACKNOWLEDGMENTS

This work was funded by the EPSRC (EP/K012568/1, EP/K012576/1, and EP/K00512X/1).

■ REFERENCES

- (1) Ewald, A. H.; Martin, R. L.; Ross, G.; White, A. H. *Proc. R. Soc. London, Ser. A* **1964**, *280*, 235–257.
- (2) *Spin Crossover in Transition Metal Compounds I–III*; Gütllich, P., Goodwin, H. A., Eds.; *Topics in Current Chemistry*; Springer-Verlag: Berlin, Germany, 2004; Vols. 233–235.
- (3) *Spin-crossover materials—properties and applications*; Halcrow, M. A., Ed.; John Wiley & Sons, Ltd.: New York, 2013; p 568.
- (4) (a) Cavallini, M. *Phys. Chem. Chem. Phys.* **2012**, *14*, 11867–11876. (b) Shepherd, H. J.; Molnár, G.; Nicolazzi, W.; Salmon, L.; Bousseksou, A. *Eur. J. Inorg. Chem.* **2013**, 653–661. (c) Molnár, G.; Salmon, L.; Nicolazzi, W.; Terki, F.; Bousseksou, A. *J. Mater. Chem. C* **2014**, *2*, 1360–1366.
- (5) Halcrow, M. A. *Chem. Soc. Rev.* **2011**, *40*, 4119–4142.
- (6) For other recent reviews see: (a) Bousseksou, A.; Molnár, G.; Salmon, L.; Nicolazzi, W. *Chem. Soc. Rev.* **2011**, *40*, 3313–3335. (b) Muñoz, M. C.; Real, J. A. *Coord. Chem. Rev.* **2011**, *255*, 2068–2093. (c) Tao, J.; Wei, R.-J.; Huang, R.-B.; Zheng, L.-S. *Chem. Soc. Rev.* **2012**, *41*, 703–737. (d) Gütllich, P. *Eur. J. Inorg. Chem.* **2013**, 581–591. (e) Gütllich, P.; Gaspar, A. B.; Garcia, Y. *Beilstein J. Org. Chem.* **2013**, *9*, 342–391. (f) Sorai, M.; Nakazawa, Y.; Nakano, M.; Miyazaki, Y. *Chem. Rev.* **2013**, *113*, PR41–PR122. (g) Guionneau, P. *Dalton Trans.* **2014**, *43*, 382–393.
- (7) Kahn, O.; Martinez, C. J. *Science* **1998**, *279*, 44–48.
- (8) Shepherd, H. J.; Gural'skiy, I. A.; Quintero, C. M.; Tricard, S.; Salmon, L.; Molnár, G.; Bousseksou, A. *Nat. Commun.* **2013**, *4*, 2607/1–2607/9.
- (9) Šalitroš, I.; Madhu, N. T.; Boča, R.; Pavlik, J.; Ruben, M. *Monatsh. Chem.* **2009**, *140*, 695–733.
- (10) Santoro, A.; Kulmaczewski, R.; Kershaw Cook, L. J.; Halcrow, M. A., submitted for publication.
- (11) Real, J. A.; Muñoz, M. C.; Faus, J.; Solans, X. *Inorg. Chem.* **1997**, *36*, 3008–3013.
- (12) (a) Moliner, N.; Salmon, L.; Capes, L.; Muñoz, M. C.; Létard, J.-F.; Bousseksou, A.; Tuchagues, J.-P.; McGarvey, J. J.; Dennis, A. C.; Castro, M.; Burriel, R.; Real, J. A. *J. Phys. Chem. B* **2002**, *106*, 4276–4283. (b) Galet, A.; Gaspar, A. B.; Agusti, G.; Muñoz, M. C.; Levchenko, G.; Real, J. A. *Eur. J. Inorg. Chem.* **2006**, 3571–3573.
- (13) Thompson, A. L.; Goeta, A. E.; Real, J. A.; Galet, A.; Muñoz, M. C. *Chem. Commun.* **2004**, 1390–1391.

(14) (a) Naggert, H.; Bannwarth, A.; Chemnitz, S.; von Hofe, T.; Quandt, E.; Tuczek, F. *Dalton Trans.* **2011**, *40*, 6364–6366. (b) Gopakumar, T. G.; Matino, F.; Naggert, H.; Bannwarth, A.; Tuczek, F.; Berndt, R. *Angew. Chem., Int. Ed.* **2012**, *51*, 6262–6266. (c) Gopakumar, T. G.; Bernien, M.; Naggert, H.; Matino, F.; Hermanns, C. F.; Bannwarth, A.; Mühlenberend, S.; Krüger, A.; Krüger, D.; Nickel, F.; Walter, W.; Berndt, R.; Kuch, W.; Tuczek, F. *Chem.—Eur. J.* **2013**, *19*, 15702–15709.

(15) (a) Palamarciuc, T.; Oberg, J. C.; El Hallak, F.; Hirjibehedin, C. F.; Serri, M.; Heutz, S.; Létard, J.-F.; Rosa, P. *J. Mater. Chem.* **2012**, *22*, 9690–9695. (b) Warner, B.; Oberg, J. C.; Gill, T. G.; El Hallak, F.; Hirjibehedin, C. F.; Serri, M.; Heutz, S.; Arrio, M.-A.; Sainctavit, P.; Mannini, M.; Poneti, G.; Sessoli, R.; Rosa, P. *J. Phys. Chem. Lett.* **2013**, *4*, 1546–1552.

(16) Pronschinske, A.; Bruce, R. C.; Lewis, G.; Chen, Y.; Calzolari, A.; Buongiorno-Nardelli, M.; Shultz, D. A.; You, W.; Dougherty, D. B. *Chem. Commun.* **2013**, *49*, 10446–10452.

(17) Zhang, X.; Palamarciuc, T.; Létard, J.-F.; Rosa, P.; Lozada, E. V.; Torres, F.; Rosa, L. G.; Doudin, B.; Dowben, P. A. *Chem. Commun.* **2014**, *50*, 2255–2257.

(18) (a) Katayama, K.; Hirotsu, M.; Kinoshita, I.; Teki, Y. *Dalton Trans.* **2012**, *41*, 13465–13473. (b) Nihei, M.; Suzuki, Y.; Kimura, N.; Kera, Y.; Oshio, H. *Chem.—Eur. J.* **2013**, *19*, 6946–6949. (c) Milek, M.; Heinemann, F. W.; Khusniyarov, M. M. *Inorg. Chem.* **2013**, *52*, 11585–11592.

(19) Trofimenko, S. *Inorg. Synth.* **1970**, *12*, 99–109.

(20) Collins, J. G.; Sleeman, A. D.; Aldrich-Wright, J. R.; Greguric, I.; Hambley, T. W. *Inorg. Chem.* **1998**, *37*, 3133–3141.

(21) Dupureur, C. M.; Barton, J. K. *Inorg. Chem.* **1997**, *36*, 33–43.

(22) McConnell, A. J.; Lim, M. H.; Olmon, E. D.; Song, H.; Dervan, E. E.; Barton, J. K. *Inorg. Chem.* **2012**, *51*, 12511–12520.

(23) Sheldrick, G. M. *Acta Crystallogr., Sect. A* **2008**, *64*, 112–122.

(24) Barbour, L. J. *J. Supramol. Chem.* **2001**, *1*, 189–191.

(25) POVRAY, version 3.5; Persistence of Vision Raytracer Pty. Ltd.: Williamstown, Victoria, Australia, 2002. <http://www.povray.org>.

(26) Dolomanov, O. V.; Bourhis, L. J.; Gildea, R. J.; Howard, J. A. K.; Puschmann, H. *J. Appl. Crystallogr.* **2009**, *42*, 339–341.

(27) Spek, A. L. *J. Appl. Crystallogr.* **2003**, *36*, 7–13.

(28) O'Connor, C. J. *Prog. Inorg. Chem.* **1982**, *29*, 203–283.

(29) (a) McCusker, J. K.; Rheingold, A. L.; Hendrickson, D. N. *Inorg. Chem.* **1996**, *35*, 2100–2112. (b) Guionneau, P.; Marchivie, M.; Bravic, G.; Létard, J.-F.; Chasseau, D. *Top. Curr. Chem.* **2004**, *234*, 97–128. (c) Marchivie, M.; Guionneau, P.; Létard, J.-F.; Chasseau, D. *Acta Crystallogr., Sect. B* **2005**, *61*, 25–28.

(30) Hunter, C. A.; Sanders, J. K. M. *J. Am. Chem. Soc.* **1990**, *112*, 5525–5534.

(31) (a) Ritter, G.; König, E.; Irlner, W.; Goodwin, H. A. *Inorg. Chem.* **1978**, *17*, 224–228. (b) Hinek, R.; Spiering, H.; Gutlich, P.; Hauser, A. *Chem.—Eur. J.* **1996**, *2*, 1435–1439. (c) Marchivie, M.; Guionneau, P.; Létard, J.-F.; Chasseau, D.; Howard, J. A. K. *J. Phys. Chem. Solids* **2004**, *65*, 17–23. (d) Craig, G. A.; Costa, J. S.; Teat, S. J.; Roubeau, O.; Yufit, D. S.; Howard, J. A. K.; Aromi, G. *Inorg. Chem.* **2013**, *52*, 7203–7209. (e) Murnaghan, K. D.; Carbonera, C.; Toupet, L.; Griffin, M.; Dirtu, M. M.; Desplanches, C.; Garcia, Y.; Collet, E.; Létard, J.-F.; Morgan, G. G. *Chem.—Eur. J.* **2014**, *20*, 5613–5618.

(32) See, for example, (a) Ksefontov, V.; Levchenko, G.; Spiering, H.; Gütllich, P.; Létard, J.-F.; Bouhedja, Y.; Kahn, O. *Chem. Phys. Lett.* **1998**, *294*, 545–553. (b) Stassen, A. F.; de Vos, M.; van Koningsbruggen, P. J.; Renz, F.; Enslin, J.; Kooijman, H.; Spek, A. L.; Haasnoot, J. G.; Gütllich, P.; Reedijk, J. *Eur. J. Inorg. Chem.* **2000**, 2231–2237. (c) Moliner, N.; Gaspar, A. B.; Muñoz, M. C.; Niel, V.; Cano, J.; Real, J. A. *Inorg. Chem.* **2001**, *40*, 3986–3991. (d) Stassen, A. F.; Grunert, M.; Dova, E.; Müller, M.; Weinberger, P.; Wiesinger, G.; Schenk, H.; Linert, W.; Haasnoot, J. G.; Reedijk, J. *Eur. J. Inorg. Chem.* **2003**, 2273–2282. (e) Money, V. A.; Carbonera, C.; Elhaik, J.; Halcrow, M. A.; Howard, J. A. K.; Létard, J.-F. *Chem.—Eur. J.* **2007**, *13*, 5503–5514. (f) Létard, J.-F.; Asthana, S.; Shepherd, H. J.; Guionneau, P.; Goeta, A. E.; Suemura, N.; Ishikawa, R.; Kaizaki, S. *Chem.—Eur. J.* **2012**, *18*, S924–S934. (g) Paradis, N.; Chastanet, G.;

Létard, J.-F. *Eur. J. Inorg. Chem.* **2013**, 968–974. (h) King, P.; Henkelis, J. J.; Kilner, C. A.; Halcrow, M. A. *Polyhedron* **2013**, *52*, 1449–1456.